Monolithic Tunable Coupled-Cavity WDM Transmitter in a Generic Foundry Platform

Weiming Yao, *Student Member, IEEE*, Giovanni Gilardi, Domenico D'Agostino, Meint K. Smit, *Fellow, IEEE*, and Michael J. Wale, *Member, IEEE*

***Abstract*— We present the monolithic integration of an extended tuning range coupled-cavity laser with traveling-wave Mach–Zehnder modulators in a low-cost generic photonic foundry platform for 10 Gb/s operation. Using an intra-cavity Michelson interferometer combined with on-chip reflectors, the coupled-cavity laser shows a tuning range of 25 nm. The modulator building blocks with optimized traveling wave electrodes exhibit efficient modulation and 8.5-GHz electro-optic bandwidth, enabling 10 Gb/s ON–OFF keying. We demonstrate error-free operation of the tunable transmitter in a full photonic circuit environment. The laser modulator combination neither requires Bragg grating formation for wavelength tuning nor additional growth steps for multiquantum-well material in the modulator section and is therefore well suited for cost effective foundry platforms specifically for low-cost applications.**

***Index Terms*— Integrated modulators, photonic integrated circuits, tunable lasers, tunable transmitter.**

I. Introduction

With the emergence of generic InP-based foundry processes photonic integrated circuits (PICs) have been made accessible to a wide range of users for plenty of applications [1]. The ability to integrate active and passive components monolithically on a single substrate combined with the generic approach to PIC design and fabrication allows for scalable, high density, high performance single chip solutions at a moderate cost [2], [3]. Tunable lasers and fast modulators have always been essential components in many PIC designs not only for the telecom and datacom areas but also in other fields such as microwave photonics or optical sensing. Monolithic integration of both devices to form a tunable transmitter has therefore been an important goal and was successfully demonstrated as early as in the '90s in form of a DFB laser integrated with an electro-absorption modulator [4]. Since then, research mainly focused on improving tuneability and operation speed by utilizing DBR lasers in conjunction with traveling-wave Mach-Zehnder modulators (MZM) [5], [6]. This has been adopted by generic III-V foundries recently so that transmitter PICs with DBR based lasers and MZMs were successfully demonstrated [7], [8]. However, formation of the Bragg gratings requires high lithographic resolution which increases the cost of the fabrication procedure. Furthermore, another epitaxial growth step in addition to the active and passive layer definition is often applied to form multi quantum-wells (MQWs) in modulator sections and to employ the Quantum-Confined Stark Effect, adding complexity to the device fabrication. For many applications that do not require ultimate performance, it is desirable to have access to tunable laser and modulator devices that can be monolithically integrated into a simple, low-cost foundry process with a minimum number of epitaxial and processing steps. One way is to substitute the Bragg grating by on-chip multi-mode interference reflectors (MIRs) [9] and use a tunable filter element such as an arrayed-waveguide-grating (AWG) for wavelength selection [10]. Although tunable multi-wavelength lasing could be achieved in this way, the devices occupy a large amount of chip space and are lacking in scalability. Another approach is to use interference between multiple cavities to obtain lasing mode tuning, as was demonstrated in [11]. Similarly, a proposed laser design based on two coupled Fabry-Perot cavities where the resulting lasing mode is determined by the overlap of longitudinal cavity modes through the Vernier effect showed promising performance without relying on a tunable grating or AWG filter [12]. By adding a wavelength selection mechanism in form of a Michelson interferometer and slightly modifying the design, an extended tuning range of 25 nm was demonstrated in these devices [13]. In this work, the two novel laser types are placed within a photonic integrated circuit environment by integrating them together with traveling-wave MZMs, thus forming a tunable, low-cost WDM transmitter device. The modulators utilize the electro-optic effect in bulk InGaAsP (Q-1.25) waveguides and are optimized for 10 Gbps on-off-keying for short-reach applications. We first present the details of the laser and modulator devices and then report on the performance characterization of the whole transmitter.

Manuscript received November 14, 2016; revised December 29, 2016; accepted January 19, 2017. Date of publication January 27, 2017; date of current version February 22, 2017. This work was supported in part by the Dutch STW ELPHI Project and in part by the SMART Photonics foundry.

W. Yao, D. D'Agostino, K. Smit and M. J. Wale are with the COBRA Research Institute, Eindhoven University of Technology, 5612 AZ Eindhoven, Netherlands (e-mail: w.yao@tue.nl; D.Dagostino@tue.nl; m.k.smit@tue.nl; m.j.wale@tue.nl).

G. Gilardi is with the Infinera Corporation, Sunnyvale, CA 94089 USA (e-mail: ggilardi@infinera.com).

Color versions of one or more of the figures in this letter are available online at http://ieeexplore.ieee.org.

Digital Object Identifier 10.1109/LPT.2017.2661200

II. Tunable Coupled-Cavity Laser

Two types of coupled-cavity lasers are discussed in this work and their respective structures are shown in the schematics in Fig. 1a and 1b. The first type which will be named the coupled-cavity laser (CCL) consists of two Fabry-Perot cavities with 940μm and 970μm length. Each cavity contains a 500μm long multi-quantum-well (MQW) gain section, emitting at 1.55μm, and a 270μm long passive phase section, based on 1.25μm bandgap quaternary material (Q-1.25). Both cavities are coupled by a novel MIR that introduces a π phase change between its input ports as described in [12]. The other side of both cavities ends in conventional on-chip

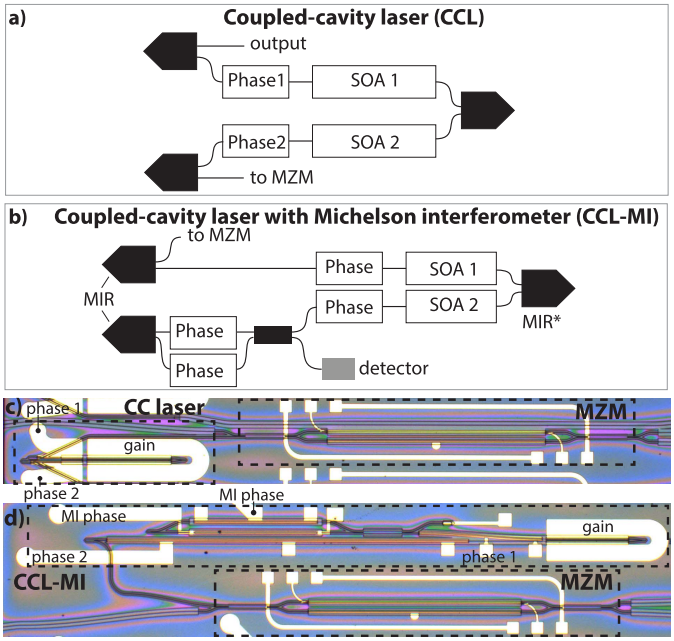

Fig. 1. Schematic structure of (a) CCL and (b) CCL-MI laser with intra-cavity Michelson interferometer. (c-d) Photograph of fabricated lasers together with traveling-wave modulator.

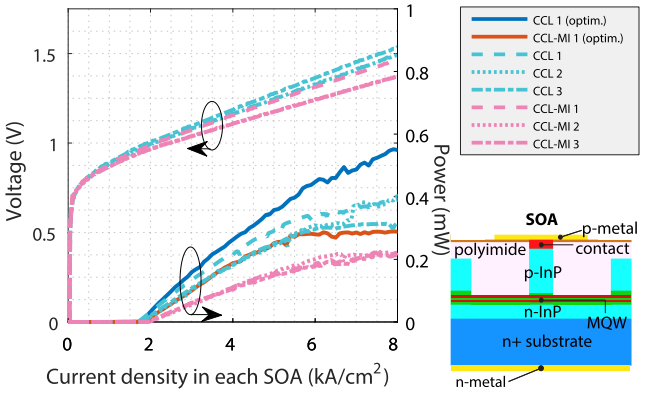

Fig. 2. LI and IV curves measured for the set of CCLs and CCL-MIs and after optimization with phase tuning sections. The output power difference between both types originates from modulator insertion loss. Inset shows schematic cross section of laser devices.

MIR mirrors that replace the cleaved facet mirrors used in previously reported devices. This allows the arbitrary placement of the laser inside a photonic circuit, improving the flexibility of the whole PIC design. The second laser type (CCL-MI) also consists of two coupled-cavities but contains a Michelson interferometer (MI) inside the second cavity. The reflective element of the interferometer is again realized by the novel MIR, introducing a π phase shift between its two input ports, thus doubling the interferometer free-spectral-range (FSR), which then acts as a tunable intra-cavity filter for the lasing mode selection of the second cavity [13]. Due to the addition of the interferometer both cavities are significantly longer: 2046 μm and 3426μm respectively. Yet, as shown in Fig. 1d, a small foot-print in the vertical direction could be retained by folding the device design appropriately. The phase tuning sections inside the MI are operated in reverse bias and have a length of 750μm whereas the phase sections outside the MI are operated with current injection. To minimize the number of bond pads, the gain sections of both cavities are electrically connected together for each laser. Previous work indicated that symmetric pumping of both gain sections results in best lasing stability and output power [12]. Both lasers are connected to traveling-wave MZMs through passive waveguides as shown in Fig. 1c and 1d. The vertical separation of the laser active section to the modulator was set to 400 µm in the CCL-MI case in order to minimize the amount of thermal crosstalk as discussed in [14], [15]. The fabrication was performed by a generic III-V foundry in a standard multi-project wafer run using a three-step, butt-joint epitaxial growth technique on n-doped InP substrate. In a first step, the 500 nm thick active material is grown, containing four InGaAsP MQWs. It is then removed in places where no gain is required and a selective area regrowth fills those with transparent Q-1.25 material, which is used for phase modulation and waveguiding purposes. A third growth step establishes the p-doped cladding material. Subsequent etching can form deep and shallow ridge waveguides with loss values of 4 and 3 dB/cm, respectively. The shallow waveguides are used for the laser and modulator sections as depicted in the insets of Fig. 2 and Fig. 5. Polyimide is used as a passivation material throughout the whole chip.

Experimental characterization of the lasers was performed with continuous-wave current injection of the gain sections through the topside p-metal and the backside n-metal and the temperature of the chip was stabilized at 20°C using water and thermo-electric cooling. The LI and IV curves for all six lasers of the fabricated PIC are shown in Fig. 2. The output power can be optimized with the phase tuning sections for both laser types, as the emitted power is maximum, when the two cavity modes perfectly align with each other. In case of the CCLs, the power was measured from the top output of the laser and in case of the CCL-MIs the values are taken after the modulators, which explains the 3 dB difference in output power. The threshold current density of the lasers lies at 1.8 kA/cm^2 (18 mA) per cavity which agrees well with values obtained from previous work on similar designs [12], [13].

The CCL laser can be tuned along 8 nm which is shown in Fig. 3c. By correctly adjusting the phase sections of the two coupled-cavities, single mode lasing with SMSR>30 dB can be achieved. Tuning occurs discretely along the longitudinal cavity modes when the current in the phase section is altered, as shown in Fig. 3a and 3b for each phase section separately. The modes of the cavity under tuning are shifted with respect to the modes of the fixed cavity, so that subsequent ones overlap and the lasing wavelength is altered. At the edge of the FSR (8.4 nm), the lasing mode reverts back to the starting wavelength, indicating a π phase change at 5 mA injection current. Both phase sections act in a complementary way, so that precise wavelength control can be established through push-pull operation. In theory, quasi-continuous tuning can be obtained with the Vernier effect in this way, if the correct phase current values are applied [16], but in experiment, it is limited by a finite amount of sweep points during the measurement.

The CCL-MI laser exhibits a total tuning range of 25 nm as depicted in Fig. 4c. This extended range is due to the MI filter,

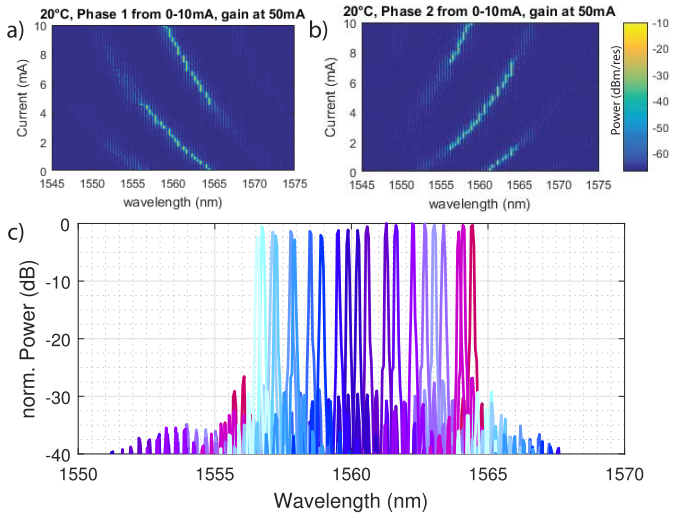

Fig. 3. Tuning map of CCL when (a) phase 1 and (b) phase 2 is varied. (c) Plot showing tuning range of CCL.

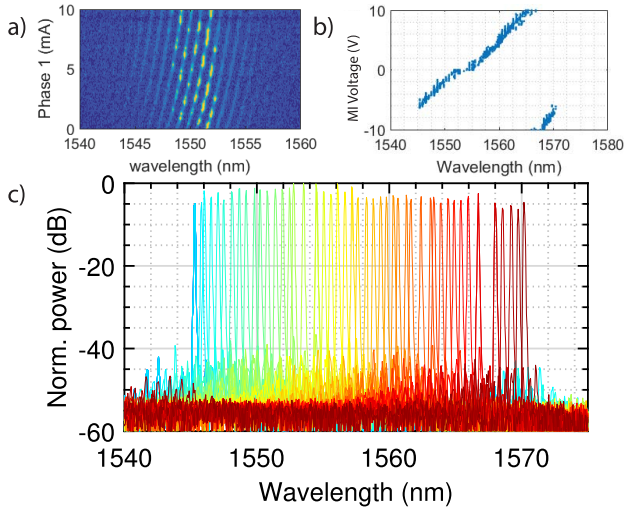

Fig. 4. (a) Fine tuning of CCL-MI laser when phase 1 is varied. (b) Coarse tuning of CCL-MI laser when MI filter is varied. (c) Plot showing tuning range of 25 nm.

whose spectral characteristics can be tuned with reverse biased phase-shifters. The extended FSR (23.6 nm) in conjunction with the gain profile leads to a better suppression of the side modes of the adjacent cavity FSR, resulting in SMSR>40 dB along the tuning range. Wavelength selection occurs through coarse tuning with the MI filter as shown in Fig. 4b, where the phase-shifters can be adjusted in a push-pull way to address a total phase shift of 2π within a voltage range of 20 V, yielding a wavelength variation of 25 nm. Fine tuning is performed afterwards with the cavity phase sections as shown in Fig. 4a. Here less current is needed for a π phase change, because the tuning sections are longer than in the case of the previous CCLs.

After inspection of the device's cross-section, it was found that the MIRs were subject to fabrication tolerances and therefore exhibit reflectivity variations up to 1.5 dB, which explains the observed output power level. Multiple mW of laser output, which have been demonstrated previously, can be expected in future fabrication runs.

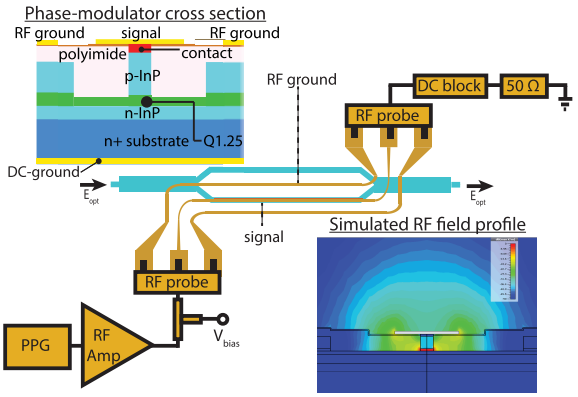

Fig. 5. Schematic structure of a single-drive traveling-wave MZM. Insets show phase-shifter cross section and simulated RF field distribution of a high-speed data signal at 10 GHz.

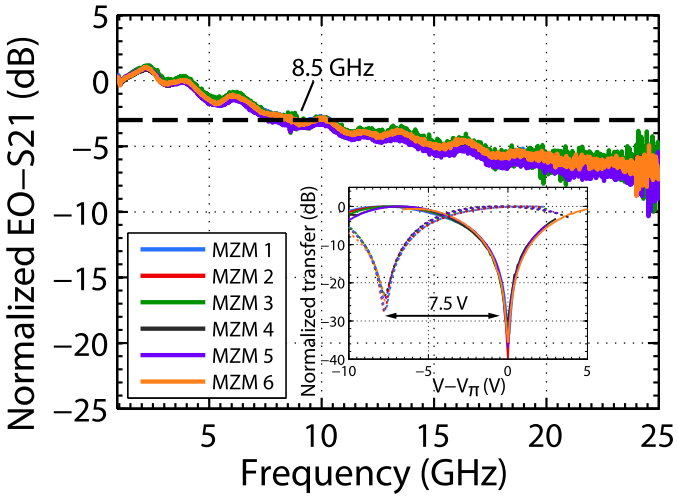

Fig. 6. Measured small-signal modulation response at $\lambda = 1550.92$nm, biasing at quadrature point and termination with 50 Ω. Inset shows DC extinction of modulator.

III. Traveling-Wave Modulator

Connected to the lasers are single-drive traveling-wave MZMs, that utilize the bulk electro-optic effect in Q-1.25 shallow etched ridge waveguides. With the proper electrode design, this type of modulator can operate at 10 Gbps OOK, being fully compatible with the low-cost platform [17]. Here, we use the single-drive scheme in order to minimize the amount of electrical connections to the driving circuit and therefore reduce its packaging complexity, but if no residual chirp is desired, a dual-drive version can be easily implemented employing a parallel push-pull scheme. The modulator cross section can be seen in the inset of Fig. 5. The phase-shifter is operated in reverse-bias, so that an electric field builds up along the depletion region of the p-i-n junction. A total length of 1.25 mm is chosen as a trade-off between modulation speed and efficiency in bulk Q-1.25 material. Static characterization at 20°C shows a V_π of 7.5 V in the inset of Fig. 6 with extinction ratio of 40 dB. The total insertion loss of the modulators has been characterized with the help of an external input waveguide, leading to the chip facet, and is below 4 dB.

The microwave design of the modulator electrode follows a compromise between electro-optic bandwidth and efficiency.

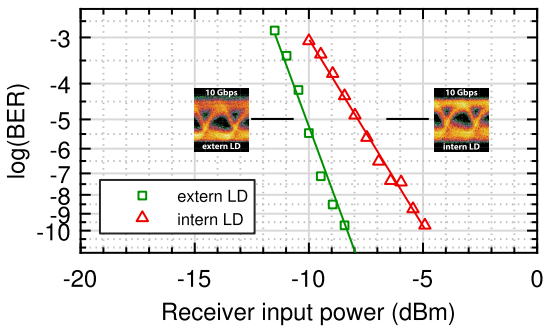

Fig. 7. BER measured at 1560.98 nm for internal and external laser. Laser settings were: 150 mA gain, 13.78 mA phase current, −11.61V MI voltage, 4.5 V peak-to-peak drive voltage.

It consists of a hybrid coplanar microstrip transmission line with 10 μm signal and 25 μm ground metal lines and a gap of 130 μm, leading to a characteristic impedance of 43 Ω with an effective microwave index of 6.9 due to the slow-wave nature of the propagation mode. The bandwidth is mainly limited by microwave attenuation in the p-doped cladding layer and the n-doped substrate and is in the order of 1.9 dB/mm. The values are obtained from full-wave EM simulations where the resulting field distribution at 10 GHz is shown in Fig. 5. The majority of the electric field is located in the core region of the optical waveguide but some parasitic field is built up from the electrode to the substrate, adding to the parasitic capacitance of the electrode.

Dynamic measurements have been performed with an Agilent N4373C lightwave component analyzer and coplanar RF probes using standard on-chip calibration techniques (short-open-load-thru on impedance standard substrate). The modulator small-signal response was measured under quadrature bias and 50 ω termination of the electrode and is shown in Fig. 6. A 3 dB bandwidth of 8.5 GHz can be observed, allowing for 10 Gbps OOK operation. Small oscillations in the measured curves are caused by electrical reflections from the slightly mismatched termination loads. Eye diagrams have been measured using a $2^{11} - 1$ long PRBS sequence that is amplified to 17 dBm and fed to the modulator electrode through RF probes. The optical eye is taken after amplification to 0 dBm with an EDFA and bandpass filtering (BW$<$1nm) its ASE noise. The measurement has been performed with an external tunable laser source and compared to the case when the on-chip tunable lasers were used. Fig. 7 shows the back-to-back bit-error rates (BER) and the resulting eye diagrams. Error-free operation can be achieved at 10 Gbps and no significant difference is observed in the eye opening comparing the external laser with the on-chip source. The transmission power penalty, in the range of 2.5 dB at 10^{-5} BER for using the on-chip laser source allows for −5 dBm receiver sensitivity. The origin of the power penalty is still under investigation but may be related to external feedback, as no isolator was used in the experiment with the PIC, whereas the external laser was a laboratory equipment containing an isolator.

IV. Conclusions

We have demonstrated, for the first time, the monolithic integration of coupled-cavity tunable lasers, based on a novel MIR reflector, with traveling-wave Mach-Zehnder modulators within a simple low-cost photonic foundry platform. Both the laser and modulator have minimum requirements on process technology and were fabricated in a multi-project wafer run without the need for Bragg gratings or additional modulator MQW layers. The results show the successful monolithic integration of both devices with full platform compatibility, preservation of tuning range and stable lasing operation. Furthermore, we demonstrate 10 Gbps error-free operation with the on-chip laser and modulator. Small footprint, flexible placement and easy scalability of this laser-modulator combination make it very promising for coming high-volume, low-cost applications such as in access networks or data centers.

References

[1] M. Smit *et al.*, "Generic foundry model for InP-based photonics," *IET Optoelectron.*, vol. 5, no. 5, pp. 187–194, 2011.
[2] G. Gilardi and M. K. Smit, "Generic Inp-based integration technology: Present and prospects (invited review)," *Prog. Electromagn. Res.*, vol. 147, pp. 23–35, Jun. 2014.
[3] M. Smit *et al.*, "An introduction to InP-based generic integration technology," *Semicond. Sci. Technol.*, vol. 29, no. 8, p. 083001, Jun. 2014.
[4] M. Goto, K. Hironishi, A. Sugata, K. Mori, T. Horimatsu, and M. Sasaki, "A 10-Gb/s optical transmitter module with a monolithically integrated electroabsorption modulator with a DFB laser," *IEEE Photon. Technol. Lett.*, vol. 2, no. 12, pp. 896–898, Dec. 1990.
[5] J. S. Barton, E. J. Skogen, M. L. Masanovic, S. P. Denbaars, and L. A. Coldren, "A widely tunable high-speed transmitter using an integrated SGDBR laser-semiconductor optical amplifier and Mach–Zehnder modulator," *IEEE J. Sel. Topics Quantum Electron.*, vol. 9, no. 5, pp. 1113–1117, Sep. 2003.
[6] P.-C. Koh *et al.*, "Ultralow power dissipation widely-tunable transmitter optical subassembly for 10 Gb/s pluggable transceivers," in *Proc. Opt. Fiber Commun. Conf. (OFC)*, Mar. 2009, p. OWJ6.
[7] K. Lawniczuk *et al.*, "InP-based photonic multiwavelength transmitter with DBR laser array," *IEEE Photon. Technol. Lett.*, vol. 25, no. 4, pp. 352–354, Feb. 15, 2013.
[8] S. Stopinski, M. Malinowski, R. Piramidowicz, M. Smit, and X. Leijtens, "Monolithically integrated 8-channel WDM reflective modulator," in *Proc. Opt. Fiber Commun. Conf. (OFC)*, Mar. 2013, p. OW4J.7.
[9] E. Kleijn, M. K. Smit, and X. J. M. Leijtens, "Multimode interference reflectors: A new class of components for photonic integrated circuits," *J. Lightw. Technol.*, vol. 31, no. 18, pp. 3055–3063, Sep. 15, 2013.
[10] M. J. R. Heck *et al.*, "Monolithic AWG-based discretely tunable laser diode with nanosecond switching speed," *IEEE Photon. Technol. Lett.*, vol. 21, no. 13, pp. 905–907, Jul. 1, 2009.
[11] Q. Chen *et al.*, "Demonstration of multi-channel interference widely tunable semiconductor laser," *IEEE Photon. Technol. Lett.*, vol. 28, no. 24, pp. 2862–2865, Dec. 15, 2016.
[12] D. D'Agostino, D. Lenstra, H. P. M. M. Ambrosius, and M. K. Smit, "Coupled cavity laser based on anti-resonant imaging via multimode interference," *Opt. Lett.*, vol. 40, no. 4, pp. 653–656, Feb. 2015.
[13] D. D'Agostino, D. Lenstra, H. P. P. M. Ambrosius, and M. K. Smit, "Widely tunable coupled cavity laser based on a Michelson interferometer with doubled free spectral range," in *Proc. Opt. Fiber Commun. Conf. (OFC)*, Mar. 2015, p. M2D.4.
[14] G. Gilardi, W. Yao, H. R. Haghighi, M. K. Smit, and M. J. Wale, "Substrate thickness effects on thermal crosstalk in InP-based photonic integrated circuits," *J. Lightw. Technol.*, vol. 32, no. 17, pp. 3061–3066, Sep. 1, 2014.
[15] G. Gilardi, W. Yao, M. K. Smit, and M. J. Wale, "Observation of dynamic extinction ratio and bit error rate degradation due to thermal effects in integrated modulators," *J. Lightw. Technol.*, vol. 33, no. 11, pp. 2199–2205, Jun. 1, 2015.
[16] J. Buus, M.-C. Amann, and D. J. Blumenthal, "Basic concepts of tunable laser diodes," in *Tunable Laser Diodes and Related Optical Sources*. Piscataway, NJ, USA: IEEE Press, 2009.
[17] W. Yao, G. Gilardi, M. Smit, and M. J. Wale, "Microwave modeling and analysis of an InP based phase shifter from a generic foundry process," in *Proc. 18th Annu. Symp. IEEE Photon. Soc., Benelux Chapter*, Nov. 2013, pp. 151–154.